On the mass-to-light ratios of fossil groups: Are they simply dark clusters?

Robert N. Proctor[1], Claudia Mendes de Oliveira[1], Renato Dupke[2,3,4],
Raimundo Lopes de Oliveira[5], Eduardo S. Cypriano[1], Eric D. Miller[6], Eli Rykoff[7]

[1] *Universidade de São Paulo, IAG, Rua do Matão, 1226, São Paulo, 05508-900, Brasil*
[2] *University of Michigan, Ann Arbor, MI, 48109, USA*
[3] *Eureka Scientific Inc., Oakland, CA 94602-3017*
[4] *Observatório Nacional, Rua Gal. José Cristino, 20921-400, Rio de Janeiro, Brazil*
[5] *Universidade de São Paulo, Instituto de Física de São Carlos, Caixa Postal 369, 13560-970, São Carlos, SP, Brazil*
[6] *Kavli Institute for Astrophysics and Space Research, Massachusetts Institute of Technology, Cambridge, MA 02139*
[7] *E. O. Lawrence Berkeley National Lab, 1 Cyclotron Rd. Berkeley CA, 94720*
Email: rproctor@astro.iag.usp.br

30 March 2011

ABSTRACT

Defined as X-ray bight galaxy groups with large differences between the luminosities of their brightest and second brightest galaxies, “fossil groups” are believed to be some of the oldest galaxy systems in the universe. They have therefore been the subject of much recent research.

In this work we present the deepest study to-date of 10 fossil group candidates with an average of 33 spectroscopically confirmed members per group. We confirm the high masses previously reported for many of fossil systems, finding masses more similar to those of clusters than of groups. We also confirm the high dynamical mass-to-light ratios reported in many previous studies, finding values as high as 700 in some systems.

While our results are consistent with previous studies in many ways, our interpretation is not. This is because, while the luminosities of the BCGs in these systems are consistent with their dynamical masses, their richnesses (total number of galaxies above some canonical value) are extremely low. This leads us to a new interpretation of fossil systems in which the large differences between the luminosities of their brightest and second brightest galaxies is simply the result the high BCG luminosities and low richnesses, while the low richnesses also explain the high mass-to-light ratios. We therefore propose that fossil systems can be characterised as cluster-like in their masses and BCG luminosities, but possessing the richnesses and optical luminosities of relatively poor groups.

If this picture is confirmed then our ideas about the formation and evolution of fossil systems will need to be entirely reformulated.

Key words: Galaxies: groups: general - galaxies: kinematics and dynamics

1 INTRODUCTION

The study of galaxy groups and clusters has become a powerful tool in many aspects of astrophysical research. From the cosmological perspective, groups and clusters mark the most over-dense regions of the matter distribution. They can therefore be used to constrain cosmological parameters such as Ω_m, σ_8 and w (the equation of state of dark energy).

From the galaxy formation and evolution perspective, the low velocity dispersions in galaxy groups result in frequent strong interactions between galaxies (i.e. tidal disruption and merging). The high velocity dispersions in clusters, on the other hand, suppress strong interactions between galaxies. However, the deeper potential wells and higher velocities in clusters mean that interactions with the ambient environment (the cluster potential and the intra-cluster medium) increase in importance, giving rise to processes such as ram-pressure stripping and strangulation (e.g. Gunn & Gott 1972; Fujita 2004; Rasmussen, Ponman & Mulchaey 2006; Kawata & Mulchaey 2008).

© 0000 RAS

Groups and clusters therefore provide an important testing ground for models of galaxy formation and evolution, as well as enabling the constraint of cosmological parameters. Consequently, there is an ongoing effort to identify and characterise clusters and groups in both the local universe and, more recently, at higher redshifts (ref).

A special class of groups/clusters, first identified by Ponman et al., (1994), are "fossil groups". These are defined as X-ray luminous structures ($L_X > 5 \times 10^{41} h_{70}^{-2}$ ergs s^{-1}) with a greater than 2 magnitude gap between the brightest and second brightest galaxies within half the virial radius (Jones et al., 2003). Fossil groups are therefore dominated by a massive central early-type galaxy surrounded by a swarm of much smaller galaxies and enclosed in a hot X-ray halo.

One suggested scenario for the formation of such systems is that, as a result of having remained relatively undisturbed for a significant fraction of a Hubble time, dynamical friction has had time to cause any large galaxies close to the central regions of the group to spiral inwards, ultimately to merge with the central galaxy (D'Onghia et al., 2005; Dariush et al., 2007). This process simultaneously increases the luminosity of the central galaxy and depletes the central regions of massive (bright) galaxies, thus creating the large luminosity gap which, by definition, characterises FGs. However, there is as yet no consensus on the formation mechanism, as Yoshioaka et al., (2004) find mass-to-light ratios in a sample of fossil groups substantially higher than those of "normal" groups and clusters. They propose instead that fossil groups represent massive galaxies that formed in low density environments where "they have not experienced significant accretion or merging".

A few previous studies have investigated the dynamical, X-ray and optical scaling relations of fossil groups (e.g. Yoshioka et al., 2004; Khosroshahi, Ponman & Jones 2007, hereafter KPJ07). They find FGs to be more X-ray luminous than non-fossil groups of the same optical luminosity, while still following the same L$_X$-T$_X$ relation. Each of these studies is at pains to point out that this is consistent with their early formation - regardless of their preferred formation mechanism.

Despite the controversy surrounding their actual formation mechanism(s), there is nevertheless a consensus that fossil groups represent ancient systems (in the sense that they accumulated their mass much earlier than non-fossil systems and have remained relatively undisturbed ever since). They therefore represent an important benchmark in the study of galaxy groups and clusters. For this reason much work has gone into identifying and characterising fossil groups (e.g. Vikhlinin et al., 1999; Mendes de Oliveira, Cypriano & Sodré, 2006; Cypriano, Mendes de Oliveira & Sodré, 2006; Khosroshahi, Ponman & Jones, 2006; KPJ07; Mendes de Oliveira et al. 2009; Dariush et al., 2010) since their identification by Ponman et al., (1994).

In this paper we present an analysis of the dynamical, X-ray and optical properties of ten fossil groups (five new and five previously reported in the literature); Our study is similar to that of KPJ07. However, due to our deeper spectroscopy, our sample comprises ∼40 galaxies per group, compared to ∼10 in KPJ07. The large number of galaxies per group in our study also allows us to look for spatio-dynamic substructure in our sample.

The paper is organised out as follows. In Section 2 we describe the sample selection, observations, data reductions and supplementary data. Section 3 details our methods of analysis. In Section 4 our results are presented and discussed. In Section 5 we summarise our results and discuss issues arising from them. Our conclusions are presented in Section 6.

Unless otherwise stated, all data presented in this work are scaled to a cosmology with Hubble constant of 70 km s^{-1} Mpc^{-1}, Ω_M=0.3 and Ω_Λ=0.7.

2 SAMPLE SELECTION, OBSERVATIONS AND DATA REDUCTIONS

2.1 Sample selection

Five of the groups reported in this paper were selected as possible fossil groups from the SDSS maxBCG[1] catalogue (Koester et al., 2007). We shall refer to these groups as the "SDSS sample". The sample was selected from low richness clusters (9<N$_{200}$ <25; see Miller et al., 2011) and was required to exhibit an i band magnitude gap of ≥2 mag between first and second ranked galaxies within 500 kpc of the group centre. The brightest group galaxy (BGG) was required to be brighter than 9×10^{10} $L_\odot$ (with the luminosity data k-corrected to z=0.25) and in the redshift range 0.1 < z < 0.15. Groups whose BGG exhibited evidence for a bright AGN at the core were excluded in order to maximise the utility of the low spatial resolution XMM-Newton follow-up that is part of the programme.

Within each group individual galaxies were then prioritised for spectroscopic observation on the Magellan Baade telescope. Prioritisation was performed by preferentially selecting galaxies within 500 kpc of the BCG and brighter than 20 mag in the r band. Despite the preference for galaxies close to the BGG, candidates were selected out to the full extent of the IMACS field-of-view (∼30 arcmin). No galaxies fainter than 21 mag in r were selected. Galaxies with g – i colour 0.1 mag redder than the red sequence identified in the maxBCG catalogue were also rejected as likely background galaxies.

A total of ∼90 galaxies were selected in this way for each group requiring two pointings (masks) per group. The success of the selection scheme is evidenced by the relatively high fraction of galaxies (≥50%) that we confirm to be at the redshift of the central galaxy. However, it should be noted that the scheme results in a sample that is neither photometrically nor spatially complete.

We also report new Gemini GMOS data for the fossil groups RX J1256.0+2556 and RX J1331.5+1108. Pre-imaging of the groups in g and i bands was carried out on 2006 February 2 and 2005 February 19, respectively. Imaging of each group consisted of 3 × 290s exposures in each waveband. Calibration to the SDSS photometric system was carried out using 4 stars in the Landolt (1992) field PG1323-086. Spectroscopic candidates were selected on the basis of

---

[1] Based on DR6 of the SDSS

their apparent magnitudes ($m_i < 21.5$ mag) and their position on the colour-magnitude diagram constructed using galaxies in the vicinity of the group (i.e. only galaxies close to, or bluer than, the red sequence visible in the colour-magnitude relation were selected). A total of 38 and 22 galaxies were selected in this way for RX J1256.0+2556 and RX J1331.5+1108, respectively.

We supplement the above samples with three other fossil groups that have been spectroscopically studied using GMOS as above to depths permitting the identification of 20–40 confirmed members: RX J1340.6+4018, RX J1416.4+2315 and RX J1552.2+2013. These have been previously reported in the literature by Mendes de Oliveira et al. 2009; Cypriano, Mendes de Oliveira & Sodré, 2006 and Mendes de Oliveira, Cypriano & Sodré, 2006, respectively. We shall refer these five groups (RX J1256.0+2556, RX J1331.5+1108, RX J1340.6+4018, RX J1416.4+2315 and RX J1552.2+2013) as the "RXJ sample"

For each group we also include, when available, spectroscopic SDSS data for the observed fields to augment both the literature and new groups. These relatively bright galaxies, which often include the central group galaxies, were generally avoided from our Magellan and Gemini observing plans in order to maximise the number of new group members identified.

It is important to note that the selection criteria for the two samples (SDSS and RXJ) differed. The SDSS sample was selected (as described above) to possess bright central galaxies in low richness groups, as well as meeting the magnitude gap criterion. The selection criteria of the RXJ sample are a little less well defined, being selected (according to Jones et al., 2003) by a "*variety of indicators*". The selection included only high X-ray luminosity groups with appropriate magnitude gaps and paying "*particular attention*" to groups with low ratios of X-ray to BCG optical luminosities and selecting "*..... system[s] dominated by a single galaxy*". These selection criteria were nominally designed to reflect the properties of the prototypical fossil group (RX J1340.6+4018) first reported by Ponman et al., (1994). We shall consider the impact of these differing selection criteria in a later section.

2.2 Observations

The Magellan Baade telescope multi-object spectroscopy of five candidate fossil groups selected from the maxBCG catalogue was carried out on the f/2 camera of the IMACS instrument in 2009 Feb. The 300 lines/mm grating was used in conjunction with the "Spectroscopic 2" filter in order to maximise the number of spectra that could be fit onto the CCD. A slit width of 1.0 arcsec was used for all galaxies. The resultant spectra covered the 4800–8000 Å spectral range at a resolution of ∼6.5 Å and a dispersion of 2.6 Å/pix (with ×2 spectral binning). The ∼30 arcmin field-of-view results in a spatial extent of >4 Mpc at the redshifts of these groups. Two 1800 s observations of two masks were carried out for each group.

The Gemini GMOS spectroscopic observations of RX J1256.0+2556 were carried out on Gemini North on 2006 June 24 (program ID GN-2006A-Q-31). Observations of RX J1331.5+1108 were carried out on Gemini North on 2005 March 7 (GN-2005A-Q-38). Observations were carried out using the R400 grating and slits of 1 arcsec width, giving a resolution of 6.5 Å over the 4000 to 8000 Å. Three exposures of 2400 s were performed. It should be noted that the field-of-view of the GMOS instrument (∼5.5×5.5 arcmin) is considerably smaller than the IMACS instrument on Magellan, resulting in a spatial extents of 1.2 Mpc and 0.5 Mpc at the redshift of RX J1256.0+2556 and RX J1331.5+1108, respectively.

2.3 Data reduction

The Magellan data (systems with prefix SDSS in Table 1) were reduced using the COSMOS pipeline provided by the Magellan consortium. However, during the analysis it was discovered that the optical map embedded in the software had not been updated after a change in the CCD configuration. This resulted in step functions in the spectral and spatial maps generated by the software. The problems in the spatial mapping are of no concern for the present work as, for our purposes, they are adequately handled by the pipeline. However, in order to compensate for the spectral distortions, it was found necessary to re-position the data on the CCDs. This process is only accurate to about 0.5 pixels (∼50 km s^{-1}). We therefore assume this value as a minimum error in individual recession velocity measures. Thereafter, reductions followed a standard procedure of de-biasing, flat-fielding, wavelength calibration (using Cu-Ar comparison-lamp exposures), sky-subtraction, cosmic-ray removal and extraction using the COSMOS pipeline[2].

Data reductions of the Gemini spectroscopic data were carried out using the IRAF Gemini package GMOS as described in Mendes de Oliveira et al. (2009). Wavelength calibrations were carried out using Cu-Ar comparison-lamp exposures. Positions and magnitudes were obtained for all objects using the SExtractor program of Bertin & Arnouts (1996).

2.3.1 Measurement of recession velocities

For the Magellan data, recession velocities were measured using the Fourier cross-correlation routine (fxcor) within IRAF. As no velocity standards were observed, a synthetic spectrum of a typical early-type galaxy was used as a template. In order to facilitate the identification of group members, the template was first redshifted by the value of the redshift of the central galaxy of the group in question, as given by the SDSS spectroscopic survey. All measured values of recession velocity are therefore with respect to the central galaxy[3].

Only cross-correlations with unambiguous peaks were

---

[2] http:/obs.carnegiescience.edu/Code/cosmos/Cookbook.html

[3] We note that the 1+z cosmological factor required in the calculation of velocity dispersion at high redshift is automatically accounted for in this approach.

accepted as valid measures. However, inspection of the spectra also revealed a number of galaxies for which unambiguous recession velocities could not be derived using fxcor, but that exhibited strong emission lines. Recession velocities for these galaxies were measured by fitting a Gaussian profile to the H_α emission line. Typical errors for both absorption and emission line errors were ∼75 km s^{-1}.

Recession velocity measurements of the Gemini data were performed using the cross-correlation technique implemented in the RVSAO package within IRAF.Several galaxy templates were employed in this analysis with results taken from the template with the strongest cross-correlation peak. Recession velocities were then converted to the rest frame of the central galaxy using:

$$V_i = \frac{cz_i - cz_0}{1 + z_0}, \tag{1}$$

where V_i is the recession velocity of the ith galaxy with respect to the BCG, which has redshift z_0.

In order to maximise the number of *new* cluster members in our sample we selected against galaxies with premeasured recession velocities in the SDSS spectroscopic survey. However, in order to check the consistency of the two data sets, we did observe 8 galaxies which were also observed in the SDSS spectroscopic survey (5 in the Magellan sample galaxies and 3 in the Gemini sample of J1256). A comparison of the derived values for these galaxies showed the SDSS values to exhibit offsets of 94 ± 35 km/sec and 59 ± 35 km/sec in the Magellan and Gemini samples respectively, giving 81± 35 km/sec for the combined sample. We therefore offset our data by 81 km/sec before introducing the SDSS spectroscopic data into our analysis.

2.4 X-ray data

The X-ray data for the five new fossil group candidates presented in this work (groups with prefix SDSS) are taken from Miller et al. (in prep). The X-ray data for the remainder of the fossil groups included in this work were taken from KPJ07. The data are shown in Table 1[4]. The Miller et al. data are derived from Chandra ACIS–S3 snapshots, while the KPJ07 data are derived from deeper Chandra ACIS–S3 observations. We note that the upper-limit of $\log(L_X)<43.46$ erg s^{-1} for the non-detection of J0906 is still well above the X-ray luminosity criterion for fossil groups ($\log(L_X)>41.7$ erg s^{-1}). This group *may* still therefore meet this criterion, and its eligibility as a fossil candidate will be reviewed in a later section.

Table 1 also shows values of R_{200} (which we take in this work to be an approximation for the virial radius). Values of R_{200} are required in both the selection process (in order to determine the luminosity gap between the first and second ranked galaxies within $0.5R_{200}$), as well as in the later analysis.

Table 1 presents both the values of R_{200} used in the selection process ($R_{200,S}$) and those derived form the X-ray temperatures also presented in the table ($R_{200,X}$), which were derived using the full cosmological form of the expression given in Helsdon & Ponman (2003):

$$R_{200,X} = 1.14\sqrt{T_X}\; h_{50}^{-1}(z) Mpc, \tag{2}$$

where $h_{50}(z) = h_{50}(\Omega_M(1+z)^3 + \Omega_\Lambda)^{0.5}$ assumes a $\Omega = 1$ universe and the 1.14 coefficient was derived from the results of the N-body/SPH simulations of Navarro, Frenk & White (1995). The values of $R_{200,X}$ so derived are given in Table 1. However, J0906 is a non-detection. Consequently, only an upper limit on its X-ray luminosity could be estimated and its X-ray temperature is unconstrained. We have therefore assumed a value of 1 Mpc for R_{200} of this group based on on its dynamical properties (see Section 4.2).

Table 1 shows clear discrepancies between the values of $R_{200,S}$ and $R_{200,X}$. In the case of the SDSS sample $R_{200,S}$ values were based on the relationship between richness and R_{200} given by Hansen et al., (2005). We shall discuss the cause of the discrepancies between $R_{200,S}$ and $R_{200,X}$ values in this sample in a later section.

For the RXJ sample (but with the exception of J1340) $R_{200,S}$ was based on relationships between L_X and kT, and kT and R_{200} (see Jones et al., 2003 for details). However, for J1256, J1416 and J1552, the ROSAT X-ray data, upon which these estimates were based, yielded X-ray luminosities (and therefore R_{200} values) significantly lower than the subsequent, higher resolution Chandra data. In the case of J1340, no value of R_{200} was quoted in the original Ponman et al., (1994) paper. We therefore estimated $R_{200,S}$ using the ROSAT X-ray luminosity given in Ponman et al., (1994), and the same equations as used in the remainder of the RXJ sample. The value is given in brackets to indicate it to be an estimate only.

Unless otherwise specified, throughout this work virial radii are taken to be the $R_{200,X}$ values given in Table 1.

In Fig. 1 we plot a comparison of the L_X–T_X relation for our fossil groups to the literature relation for "normal" systems. In this figure normal groups are shown as black dots (Osmond & Ponman, 2004) and normal clusters as red dots (Wu, Xue & Fang, 1999). The figure shows the fossil groups to be generally consistent with normal systems. However, we note that a significant number of the fossil groups exhibit values consistent with *clusters* rather than groups. However, there are four systems with group-like X-ray properties. Interestingly, these appear to possess slightly low temperatures for their luminosities when compared to normal groups. We shall comment further on these trends in a later section.

3 OPTICAL ANALYSIS

In this section we detail each of the elements of our analyses of the spectroscopic and photometric data.

---

[4] Full galaxy identifiers are given here and shown in Table 1, but throughout the remainder of this paper we shall refer to them by abbreviated identifiers in the text (e.g. J0906, J1256, etc).

Table 1. For groups with prefix SDSS (the SDSS sample), X-ray data are the Chandra data of Miller et al. (2011). For the systems in the RXJ sample the Chandra data of KPJ07 are presented. X-ray luminosities and temperatures are specified for an aperture equal in size to R_{200}. The values of R_{200} used in the selection of the target systems ($R_{200,S}$) are shown (see text). Values derived from the X-ray data ($R_{200,X}$) are also presented. For SDSS J0906+0301, which was undetected in the X-ray, the $R_{200,X}$ is assumed to be 1.0 Mpc based on its dynamical properties (See Section 4.2). In all other cases $R_{200,X}$ was calculated from the X-ray temperature using Equation 2.

Group	z	$\log(L_X)$ (erg s^{-1})	kT_X (keV)	$R_{vir,S}$ (Mpc)	$R_{vir,X}$ (Mpc)
SDSS J0906+0301	0.1359	<43.29	–	0.66	(1.0)*
SDSS J1045+0420	0.1539	44.01	2.47	0.76	1.19
SDSS J1136+0713	0.1030	43.59	2.64	0.86	1.26
SDSS J0856+0553	0.0939	43.92	2.73	0.83	1.29
SDSS J1017+0156	0.1177	42.99	2.13	0.74	1.12
RX J1256.0+2556	0.2327	43.70	2.63	0.69	1.18
RX J1331.5+1108	0.0802	42.32	0.81	0.71	0.71
RX J1340.5+4017	0.1719	42.72	1.16	(0.75)*	0.81
RX J1416.4+2315	0.1381	44.23	4.00	0.93	1.52
RX J1552.2+2013	0.1357	43.78	2.85	0.83	1.29

*Assumed value.

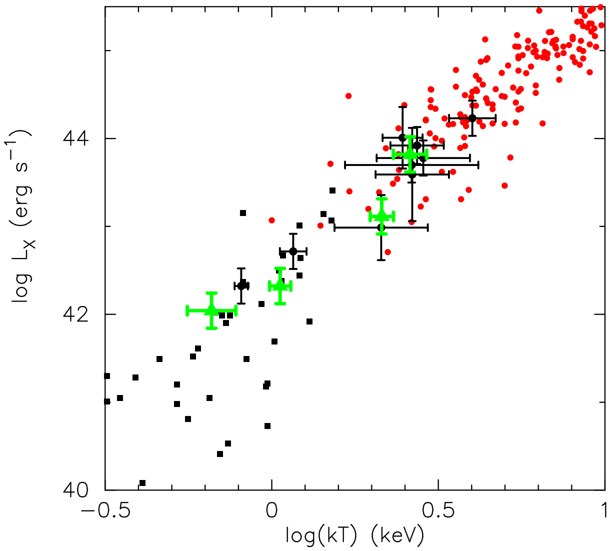

Figure 1. Fossil groups are plotted in the L_X–T_X plane and compared to literature values for "normal" systems. Literature values for normal clusters (Wu, Xue & Fang, 1999) are shown as red dots, while literature values for normal groups (Osmond & Ponman 2004) are shown as black dots. Fossils taken from KPJ07 are shown as green squares. The fossil groups analysed in this work are shown as black dots (with error bars).

3.1 Group velocities and velocity dispersions

In this section we detail our estimates of group velocities, velocity dispersions and dynamical 'virial radii (i.e. $R_{200,dyn}$) of the fossil groups.

The average velocity of the group was also calculated as:

$$RV_{group} = \frac{\Sigma V_i}{N} \pm \frac{\sigma_{200}}{\sqrt{N}}\ kms^{-1}, \qquad (3)$$

where V_i is the recession velocity of the ith galaxy within R_{200} and N is the total number of non-BCG galaxies within R_{200} (the BCG is excluded from this calculation). The offset of the BCG with respect to the group average (ΔRV_{BCG}=RV_{BCG}-RV_{group}) was then calculated (Table 2). The velocity dispersion (σ_{200}) of each group was estimated from the recession velocities by:

$$\sigma_{200} = \sqrt{\frac{\Sigma(V_i - RV_{group})^2}{N-1}} \pm \frac{\sigma_{200}}{\sqrt{2(N-1)}}\ kms^{-1}, \qquad (4)$$

Both of the above definitions require an estimate of R_{200}. For these estimates, and generally throughout this work, we use the values derived from the X-ray temperature as described in Section 2.4 and given in Table 1. However, for comparison purposes we also make virial radius estimates based on the observed velocity dispersion (which we shall refer to as *dynamical* virial radius).

3.2 Dynamical virial radii

Dynamical virial radii can be estimated from kinematic data using expressions which express the virial radius as being proportional to the velocity dispersion. From the virial theorem, Carlberg et al., (1997) derived an expression for R_{200}:

$$R_{200,dyn} = \frac{\sqrt{3}\sigma_{200}}{10H(z)}\ Mpc, \qquad (5)$$

where σ_{200} is the velocity dispersion of galaxies within R_{200} as defined above, and H(z) is the Hubble constant at redshift of the group. Alternatively, Girardi et al (1998) use both virial theory *and* observational data to derive an expression for the virial radius (at unstated over-density):

$$R_{vir,dyn} = \frac{0.2\sigma_{200}}{H_0}\ Mpc, \qquad (6)$$

Both of the above equations are directly proportional to the velocity dispersion, and differ only in the constants of proportionality (with the Girardi et al (1998) values larger by a factor of ∼15%). We therefore use Equation 5 above for estimates of the dynamical virial radii and leave it to the reader to apply the ∼15% offset if the Girardi et al (1998) values are required.

3.3 Dynamical masses

We also make estimates of the mass within R_{200} of each group or cluster. These are calculated using the expression (Ramella et al. 2004):

$$M_{200} = \frac{3}{G}\sigma_{200}^2 R_{200,X}, \tag{7}$$

which can be expressed in the more convenient form:

$$M_{200} = 6.975 \left(\frac{\sigma_{200}}{1000\ kms^{-1}}\right)^2 \left(\frac{R_{200,X}}{1\ Mpc}\right) \times 10^{14}\ M_\odot. \tag{8}$$

where $R_{200,X}$ is calculated using Equation 2. We use the X-ray derived radius, rather than those derived from the velocity dispersion in order to avoid the mass estimate being simply proportional to σ_{200}^3.

3.4 Total optical luminosities

Part of our analysis considers the total optical luminosities of the groups. For the RXJ sample, we imitate the KPJ07 procedure of simply adding the optical luminosities of all the identified group members. Since our data probe significantly further down the luminosity function (with an average of 27 galaxies per group compared to 10 galaxies per group in KPJ07) our total optical luminosities are considerably more robust.

For the SDSS sample, for which the selection functions and completeness were estimated during the construction of the composite luminosity function, we estimate the total optical luminosities using completeness-corrected data.

Finally, for the purposes of comparison, data for normal systems were taken from Osmond & Ponman (2004) and Girardi et al., (2004). However, we note that, as is the case for all the normal samples used in this work, the data were not specifically selected to possess low m_{12} values. These samples *may* therefore contain systems that we would consider fossil systems. However, given the relative rarity of fossil systems, such contamination of the normal samples is expected to be small.

3.5 Composite luminosity function

The spectroscopy obtained for the fossil candidates in this paper studied using the Magellan telescope (i.e. the SDSS sample) covers a significant radial extent in each system (i.e $>R_{200}$). This allows the accurate determination of the luminosity function (LF) of galaxies within R_{200} in these systems. Although a few determinations of the luminosity function of individual fossil groups has been attempted in the literature (Mendes de Oliveira et al. 2006 and 2009, for J1552 and J1340 and Cypriano et al. 2007 for J1416) these were within radii smaller than $0.5\times R_{200}$. This is therefore the first determination of the LF of fossil groups which include more than 30 galaxies per group and reach out to R_{200}.

To calculate the LF of each group, we considered all galaxies inside a projected (circular) area with radius corresponding to R_{200} of that group. This requires the determination of the selection function $S(m')$ in each group in order to estimate the completeness of the spectroscopy. This was done using the following equation:

$$S(m') = \frac{\#GAL_z(m')}{\#GAL(m')}\ , \tag{9}$$

where $\#GAL_z(m')$ is the total number of galaxies with known spectroscopic redshifts, being member galaxies or not, and $\#GAL(m')$ is the total number of galaxies in the region as identified via photometry (from SDSS), in both cases for galaxies with magnitude m such that $\mid m - m' \mid < \Delta m$. Membership to the group was defined in the velocity range within 2000 km/s from the velocity of the central galaxy and within R_{200} of the position of the central galaxy. Then the LF is defined by:

$$LF(m') = \frac{\#GAL_{z,grp}(m')}{S(m')}\ , \tag{10}$$

where $\#GAL_{z,grp}(m')$ is the number of member galaxies as determined by spectroscopy.

Thus, the individual LF for each group in a given band was obtained by simply dividing the number of galaxies in each bin of absolute magnitude by the completeness fraction. The second step was then to construct the composite LF by averaging, bin per bin, the individual LFs of each of the five groups for each band g, r, and i.

Finally the galaxy distributions were fitted by the Schechter function (Schechter 1976).

4 RESULTS

In this section we detail the results of our analysis. We begin by considering the results of our kinematic analysis.

4.1 Recession velocities

The distributions of the recession velocities of galaxies within ∼3 Mpc of the central galaxy are shown in Fig. 2. This figure shows that the majority of the groups exhibit recession velocity distributions that are clearly delineated, and near symmetric about zero velocity (i.e. the average velocity of the group). However, there are indications of skew distributions and gaps in the recession velocity distributions in a few cases. Other possible signs of disturbance or background contamination considered were large offsets in BCG velocity (Table 2) and spatial groupings of galaxies with similar recession velocities, In order to measure gaps and skewness we preformed an analysis using the ROSTAT software of Beers et al (1990). The results of this analysis were then combined with the BCG velocity offsets and a visual inspection for spatial groupings. In three cases (J1017, J1256 and J1416) the groups exhibited positive signs from three of the four criteria listed above. We therefore take these groups as being the most likely to be either contaminated by foreground/background structures or out of equilibrium (i.e. are unvirialised). These groups were therefore used to test the possible affects of these apparent irregularities on our derived velocity dispersions and dynamical virial radii.

Fig. 3 shows the spatial distribution of member galaxies of the three groups identified above. Circles representing R_{200} are shown. Unfortunately, even with the increase in the numbers of spectroscopically confirmed members compared to previous studies, the incomplete spatial coverage of our

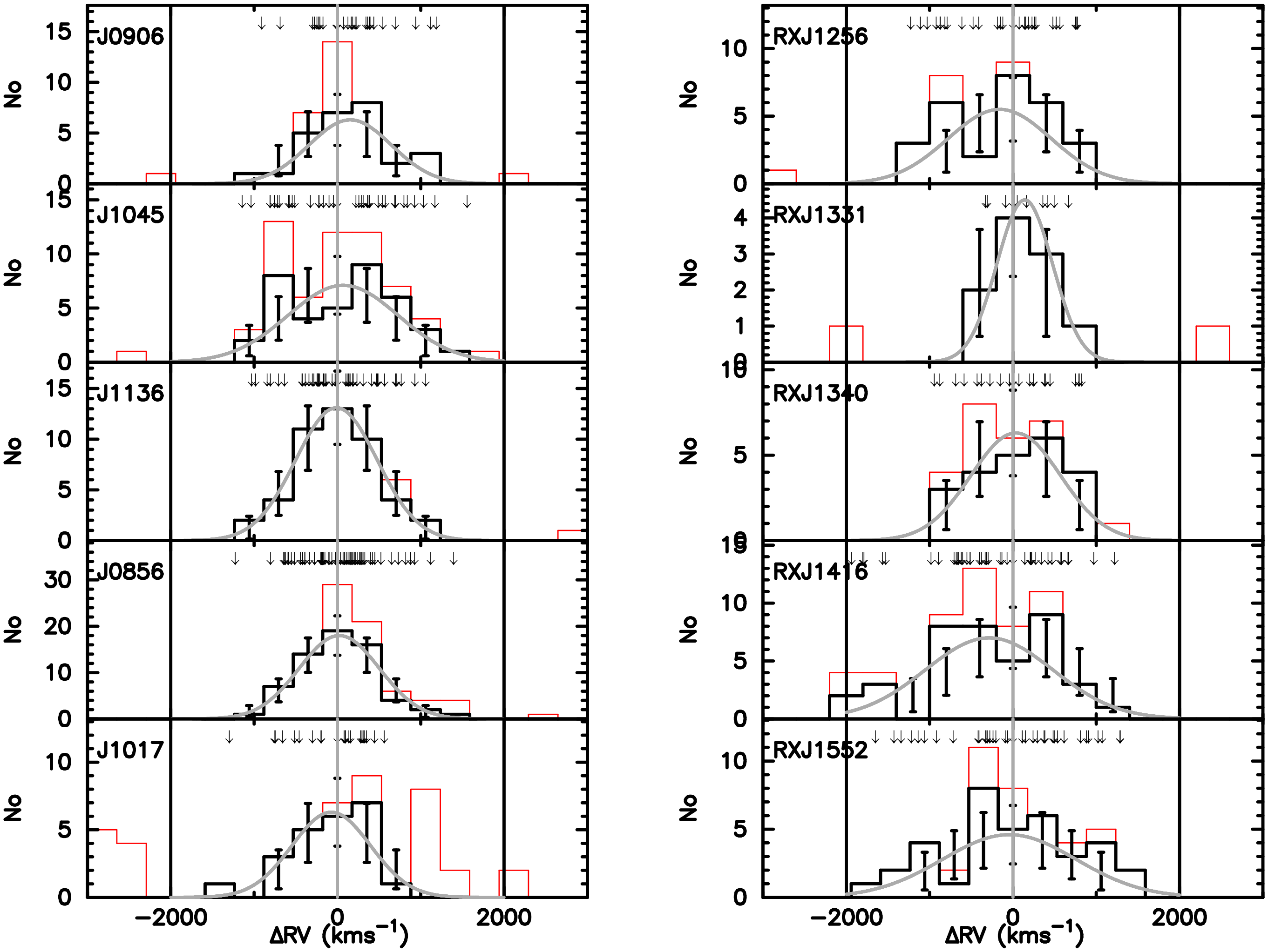

Figure 2. Distributions of recession velocities about the average group velocity. Arrows mark the recession velocities of individual galaxies. Vertical black lines represent the 2000 km s^{-1} velocity limit of group members applied to all groups. Vertical grey lines represent the velocities of the BCG in each group (ΔRV_{BCG} ; Table 2). Histograms in black include all member galaxies within the R_{200}. Red histograms show galaxies outside the velocity or radius limits. Gaussian distributions matching the recession velocity distributions (i.e assuming the velocity dispersions listed in Table 2) are shown as grey lines with Poisson errors to aid in assessing the significance of apparent velocity substructure. Significant asymmetries and/or discontinuities are visible in the distributions of J1017, J1256 and J1416.

Table 2. Dynamical data derived within R_{200}. The table shows the number of galaxies within R_{200}. (n), the estimated velocity dispersions and the offset of the BGG velocity with respect to the group average (ΔRV_{BCG}). R_{200} and masses estimated from Equations 5 and 7 are also presented. Errors in σ and ΔRV_{BCG} were calculated according to Equations 4 and 3 and were propagated through Equations 5 and refmass for R_{200} and M_{200}.

Group	n	σ (km s^{-1})	ΔRV_{BCG} (km s^{-1})	$R_{200,dyn}$ (Mpc)	$\log(M_{200})$ ($M_\odot$)
SDSS J0906	25	506±72	-154±103	1.17±0.16	14.25±0.21
SDSS J1045	38	664±77	-69±109	1.52±0.18	14.58±0.13
SDSS J1136	45	490±52	11±74	1.15±0.12	14.30±0.22
SDSS J0856	63	478±43	-24±61	1.13±0.11	14.26±0.16
SDSS J1017	23	474±71	73±101	1.11±0.17	14.23±0.29
RXJ J1256	28	622±84	159±120	1.37±0.19	14.50±0.40
RXJ J1331	10	338±77	-142±111	0.80±0.18	13.74±0.25
RXJ J1340	22	537±82	-34±117	1.22±0.19	14.21±0.10
RXJ J1416	40	815±87	285±124	1.89±0.20	14.85±0.15
RXJ J1552	35	803±96	43±138	1.86±0.23	14.76±0.28

data results in it still being insufficient for a full "friends-of-friends" type of analysis. In this section we therefore simply test the likely impact of potential substructures on our derived parameters in the three systems including or excluding them from our analysis.

4.1.1 J1017

In the case of J1017, there are a significant number of galaxies with high recession velocities (>900 km s^{-1}) located just outside R$_{200}$. Examination of Fig. 3 shows them to be located to the north-east and south and south-west of the group in a configuration which suggests that these galaxies are unlikely to be group members under the assumption that the group is virialised. However, to test for the impact of including these galaxies in our kinematic measurements, we re-calculated the velocity dispersion and ΔRV$_{BCG}$ including these galaxies. The effect was to increase the measured velocity dispersion from 474±71 to 643±88 km s^{-1} (an increase in log σ of 0.13 dex). Comparison of the dynamical R$_{200}$ (as defined in the previous section and given in Table 2) with the X-ray derived value (Table 1) shows almost perfect agreement. Therefore, the dynamical R$_{200}$ that would be derived from the increased value of velocity dispersion when the outlying galaxies are included would exceed the X-ray derived value by nearly 40%. Their inclusion also results in a significant decrease in ΔRV$_{BCG}$, with the value going from +73±101 km s^{-1} to –129±125 km s^{-1}. Therefore, while we can draw no firm conclusions, the data suggest that these high radius, high recession velocity galaxies are not part of the virialised system.

4.1.2 J1256

For J1256 we see an apparent excess of low recession velocity galaxies (Fig. 2). Examination of Fig. 3 shows that these galaxies all lie on one side of the group. Indeed, the group is remarkably reminiscent of the "bimodal" clusters reported in Maurogordato et al. (2010). The BCG also exhibits a large positive recession velocity with respect to the group average of (ΔRV$_{BCG}$; Table 2). We therefore again re-calculated the velocity dispersion and dynamical R$_{200}$, this time excluding galaxies with absolute recession velocities less than –800 km s^{-1}. This resulted in a velocity dispersion of 449±70 km s^{-1} and a ΔRV$_{BCG}$ of –115±100 km s^{-1}. The reduction in velocity dispersion of 28% (0.14 dex in log σ) results in a reduction in the dynamical R$_{200}$ such that it becomes 20% lower than the X-ray derived value rather than the 16% over-estimate of the value given in Table 2. We are therefore unable to definitively state whether these objects are part of the virialised structure on the basis of the velocity dispersion measurements. In addition, while the large positive ΔRV$_{BCG}$ is eliminated, its replacement by the relatively large negative value means that no firm conclusions can be drawn from this parameter either. However, examination of the X-ray contours (Fig. 4) of this group indicates no obvious sign of substructure associated with the overall projected location of the highly blueshifted galaxies. In fact, the X-ray isophotes seem to show an elongated substructure towards the N-NE, consistent with some dynamical turmoil, so that the sub-system of velocity outliers may be the results of the previous interaction with another group and the

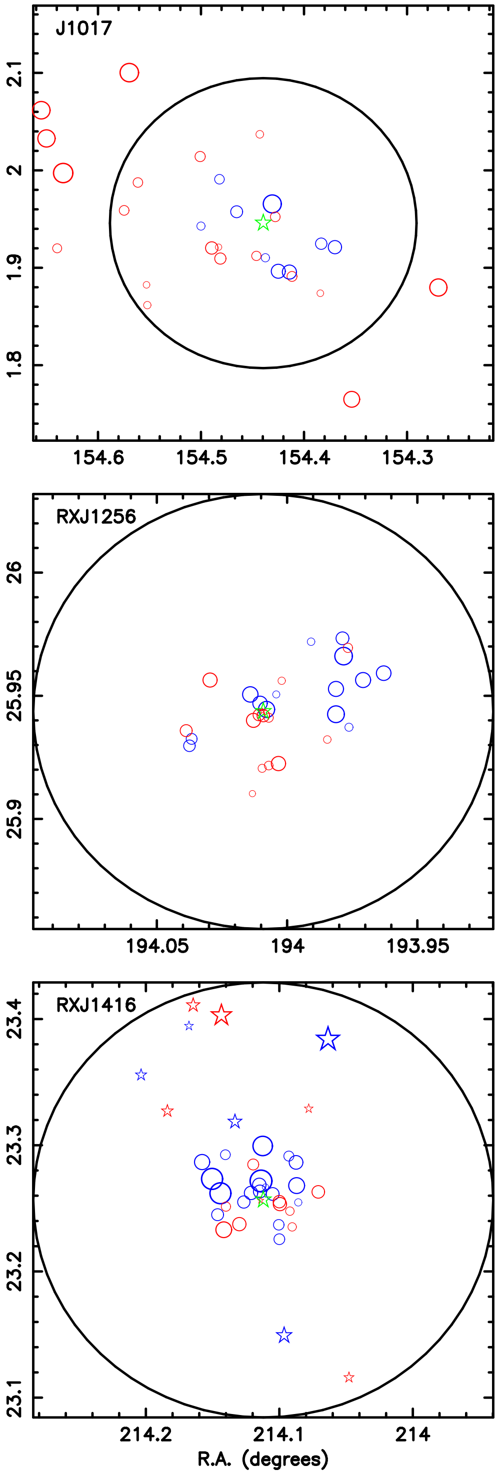

Figure 3. The spatial distributions of galaxies with recession velocities within 2000 km s^{-1} of the BGG (green star) are shown. The symbol colour indicates the *sense* of the recession velocity with respect to the BGG (red for redshift, blue for blueshift). Symbol size denotes the *magnitude* of the recession velocity with large symbols representing greater absolute velocities. Stars identify galaxies whose recession velocities were taken from the SDSS spectroscopic catalogue. Solid circles mark the R$_{200}$ radius.

system may not be fully virialised. A more complete study of this group is necessary to confirm these findings.

We also note that a close examination of the central galaxy of this system reveals two extremely nearby (on the plane of the sky), relatively bright galaxies that have not to-date been examined spectroscopically (either by us or the SDSS), and whose membership therefore remains untested. The brighter of these two galaxies is only 1.83 mag fainter in the r band than the central galaxy.

4.1.3 J1416

In J1416 we see a substantial collection of low recession velocity galaxies in Fig. 2 which are separated in redshift space from the remainder of the group by a significant gap. Examination of Fig. 3, once again, shows all the low-z galaxies to lie on one side of the group, again reminiscent of the "bimodal" clusters reported in Maurogordato et al. (2010). The group also exhibits the largest ΔRV_{BCG} in our sample. We therefore re-calculated the velocity dispersion and dynamical R_{200}, this time excluding galaxies with absolute recession velocities less than –1400 km s^{-1}. Once again, we find the large ΔRV_{BCG} to be eliminated (becoming $+74\pm98$ km s^{-1}), and the velocity dispersion to be reduced to 560 ± 68 km s^{-1} (a reduction of 0.16 dex in log σ). The dynamical R_{200} is therefore reduced from 16% greater than the X-ray derived value to 15% lower – again inconclusive. However, in this case, the X-ray profile also exhibits signs of disturbance in the sense that it is extended along the same axis as the kinematic substructure (Fig. 4). On balance the data therefore suggest that this group is subject to an going interaction/merger.

Evidence for merging is also present in the X-ray spectral analysis. J1416 is the hottest and most luminous fossil group known, with gas temperatures reaching 4 keV! It has, at larger scales, a temperature decline seen with XMM-Newton. As shown by Khosroshahi et al. (2006), this unusual fossil group has a temperature "spike" ~200 kpc from the center, followed by a strong temperature decline at r>200 kpc. This spike could be due to azimuthal temperature substructures in the inter-galactic medium. The cooling time of 5 Gyr measured for this system is significantly below the Hubble time for regions with the central 150 kpc (Khosroshahi, et al., 2006), but the expected level of cooling is not observed, implying that some extra source of gas heating is in effect, maybe shock heating due to merging.

To summarise, while there are hints of substructure in the spatial and kinematic data of a number of systems, the relatively low numbers of confirmed members and poor spatial coverage of our data preclude definitive statements about the dynamical status of these systems. We have therefore simply estimated the magnitudes of the effects such substructure might have on our derived parameters for the three most obvious potential cases, and continue to use the values derived from *all* galaxies within R_{200} throughout the this work. Clearly, follow-up observations of these systems to improve the spatial coverage and depth of spectroscopically confirmed memberships are highly desirable.

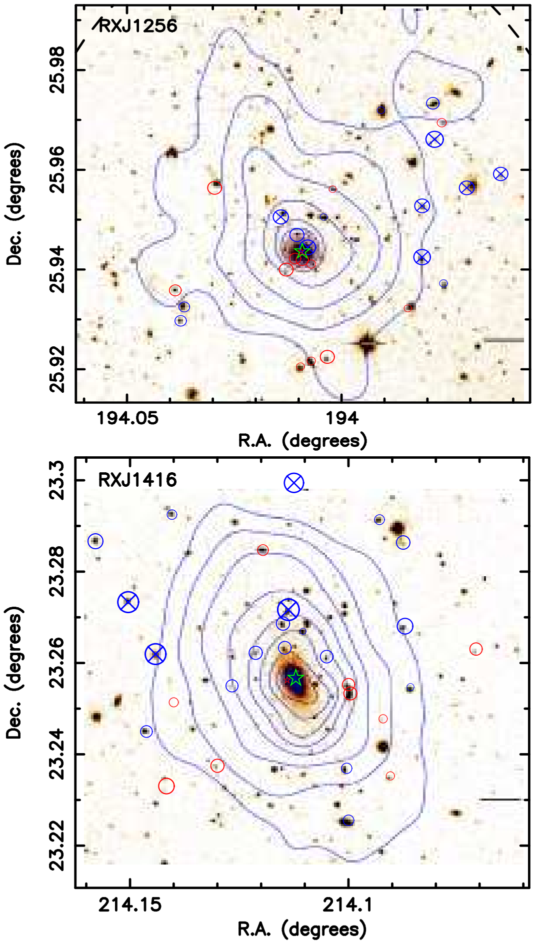

Figure 4. Our recession velocity data for J1256 and J1416 are overlayed on Chandra X-ray contours from KPJ07.

4.2 Dynamical properties

The dynamical properties (velocity dispersions, average group velocities, dynamical R_{200} values and masses) are presented in Table 2.

A comparison of our velocity dispersion results with those of KPJ07, for the four systems common to both studies, shows them to be consistent, with our results, with an offset and rms of 54 and 104 km s^{-1} with respect to the KPJ07 results. These are easily within 1σ in all cases. Comparison of the log(mass) estimates are also consistent with our results exhibiting an offset and rms of -0.02 and 0.23 dex, respectively. Comparison of the dynamical R_{200} with the X-ray derived values given in Table 1 shows good agreement, with the dynamical values on average 0.21 Mpc (18%) larger than the X-ray values with an RMS scatter of 0.20 Mpc (18%). Use of the Girardi et al (1998) expression (Equation 6) would have resulted in values ~15% larger still.

A striking feature of these dynamical measures is the magnitude of the velocity dispersion and associated mass estimates. The derived masses are, in all but one case, greater than 10^{14} $M_\odot$. These masses are more consistent with poor *clusters* than with groups – in accord with the trend suggested by the X-ray luminosities and temperatures (Section 2.4). It should be noted that the two systems with the lowest masses (J1331 and J1340) are the systems identified as possessing low X-ray temperatures and luminosities in Fig. 1. The data therefore indicate a strong correlation between dynamical and X-ray properties. We therefore next consider the scaling relations that relate the various parameters of interest in detail.

4.3 Scaling relations

In this section we examine the scaling relations that relate dynamical, X-ray and optical properties of groups and clusters. The optical data are presented in Table 3.

The results of our analysis are shown in Fig. 5. In this figure the data from the present work are shown as black dots with error bars. We also include the data for three fossil groups from KPJ07. These are shown as green dots with error bars.

The figure also shows values for normal groups and clusters from the literature. The sources for normal groups were taken from the GEMS project of Osmond & Ponman (2004), supplemented in the L_r–σ plot by groups from the study of Girardi et al., (2002). Cluster data were taken from Girardi et al., (2002) and were supplemented by data from Wu, Xue & Fang (1999) and Zhang et al., (2010). It is worth recalling that the "normal" samples may, in fact, contain some fossil systems, as these were not expressly excluded during the construction of these samples.

All literature values were converted to the H_0=70 km s^{-1} Mpc^{-1}, Ω_M=0.3, Ω_Λ=0.7 cosmology used throughout this paper. Where necessary, optical luminosities were converted to the r band using the values given in Section 4.4. The solar luminosities assumed are also given in Section 4.4.

The trend noted in the L_X–T_X plot for the majority of the fossil groups to be more similar to galaxy *clusters* than groups is evident in the plots of L_X–σ and T_X–σ of Fig. 5. We therefore find that all three of these commonly used proxies for mass are in accord, indicating that all the systems in our sample possessing masses $\sim 10^{14}$ $M_\odot$, or greater. We note that the group that was a non-detection in the X-ray (J0906) has a velocity dispersion of >500 km s^{-1} (log $\sigma \sim$ 2.7). For this system to be consistent with our other data we should expect J0906 to possess a log L_X $\sim$ 43.0. The upper limit of log L_X $\sim$ 43.3 therefore does not preclude this system from following the same scaling relations as the remainder of our sample.

However, a severe mismatch with cluster data is evident in the L_r–σ plot, with the fossil groups exhibiting r band luminosities ∼0.5 dex lower than clusters of the same velocity dispersion. Examination of the L_X–L_r plot of Fig. 5 (top right) shows the fossil groups to lie on the outer envelope of the locus of normal groups. This trend has been noted in previous works and interpreted as either a X-ray luminosity excess (e.g. KPJ07) or an optical luminosity deficit (e.g. Voevodkin et al., 2010). Considering the plots with velocity dispersion, it is our conclusion that the effect must, in fact, be an optical luminosity deficit. Indeed, we note that, if we compensate for the ∼0.5 dex deficit in L_r suggested by the L_r–σ plot, then the fossil groups would fall in the cluster region of the L_X–L_r plot.

The disparity in r band luminosity is harder to discern in the T_X–L_r plot. However, we note that the displacement of the fossil group data points by the ∼0.5 dex suggested by the L_r–σ plot leaves most of the fossil groups consistent with the trends shown by normal cluster-like systems. There are however two notable exceptions - J1331 and J1340 (the two systems with the lowest X-ray temperatures). Displacement of these two systems by such a large amount would clearly leave them in a region of the T_X–L_r plane that is unoccupied by normal systems. We note that these groups were also amongst those identified in Fig. 1 as exhibiting low T_X for their L_X. It is therefore possible that these two systems represent a separate, distinct population (i.e. following different scaling relations) from their more massive counterparts. Clearly, an expansion of the data set at low masses (low L_X, T_X) is highly desirable to address this point.

The disparity in r band luminosity between the majority of the fossil groups and normal systems of the same mass indicates that the mass-to-light ratios of the fossil groups are ∼3 times larger than normal systems of the same mass. This is demonstrated in Table 3 and Fig. 6, in which our mass and mass-to-light values (determined within $R_{200,X}$) are compared to the values for normal systems from Girardi et al., (2002). The Girardi et al. values were estimated within $R_{vir,dyn}$ (Equation 6) and are therefore well matched to our data. It is evident from Fig. 6 that the fossil groups lie on or above the highest mass-to-light ratios exhibited by normal systems. It is also interesting to note that the two low-mass fossil systems (J1331 and J1340) also possess high mass-to-light ratios. Therefore, even if these systems do signal the existence of a distinct low-mass population, this too would seem to possess high mass-to-light ratios.

We note that, until this point, our findings (including masses and total luminosities for the five overlapping systems) are in good accord with KPJ07. It is therefore perhaps a little surprising that our estimates of mass-to-light ratio are not. This can be seen by comparing our Fig. 6 with their M/L–Mass plot (their Fig. 10), which also compares the fossil systems with the Girardi et al., (2002) data for normal systems. However, it appears from the KPJ07 plot that the values presented for mass are those within R_{500} (their Table 2), rather than within R_{200} (their Table 3). It also appears that they used M_{500} in the estimation of M/L values. Since the both the total luminosities and the Girardi et al., data to which they compare are estimated within R_{200} the reasons for this choice are not clear. Therefore, we simply note that all quantities involved in the construction of our Fig. 6 are measured with $R_{200,X}$.

To summarise; our consideration of the scaling relations of fossil groups indicate that the most important parameter differentiating the fossil sample from normal systems is their optical luminosity, with Fig. 6 demonstrating that fossil systems possess mass-to-light ratios approximately three times that of normal systems of the same mass. This corresponds to a deficit of *twice* the *total* observed luminosity (including the bright BCGs). Such deficits clearly can not be explained simply by the absence of a few bright galaxies and are certainly *not* predicted by the galactic cannibalism paradigm for the formation of the large luminosity gaps. We must therefore consider the optical properties of the sample in more detail if we are to properly characterise these systems.

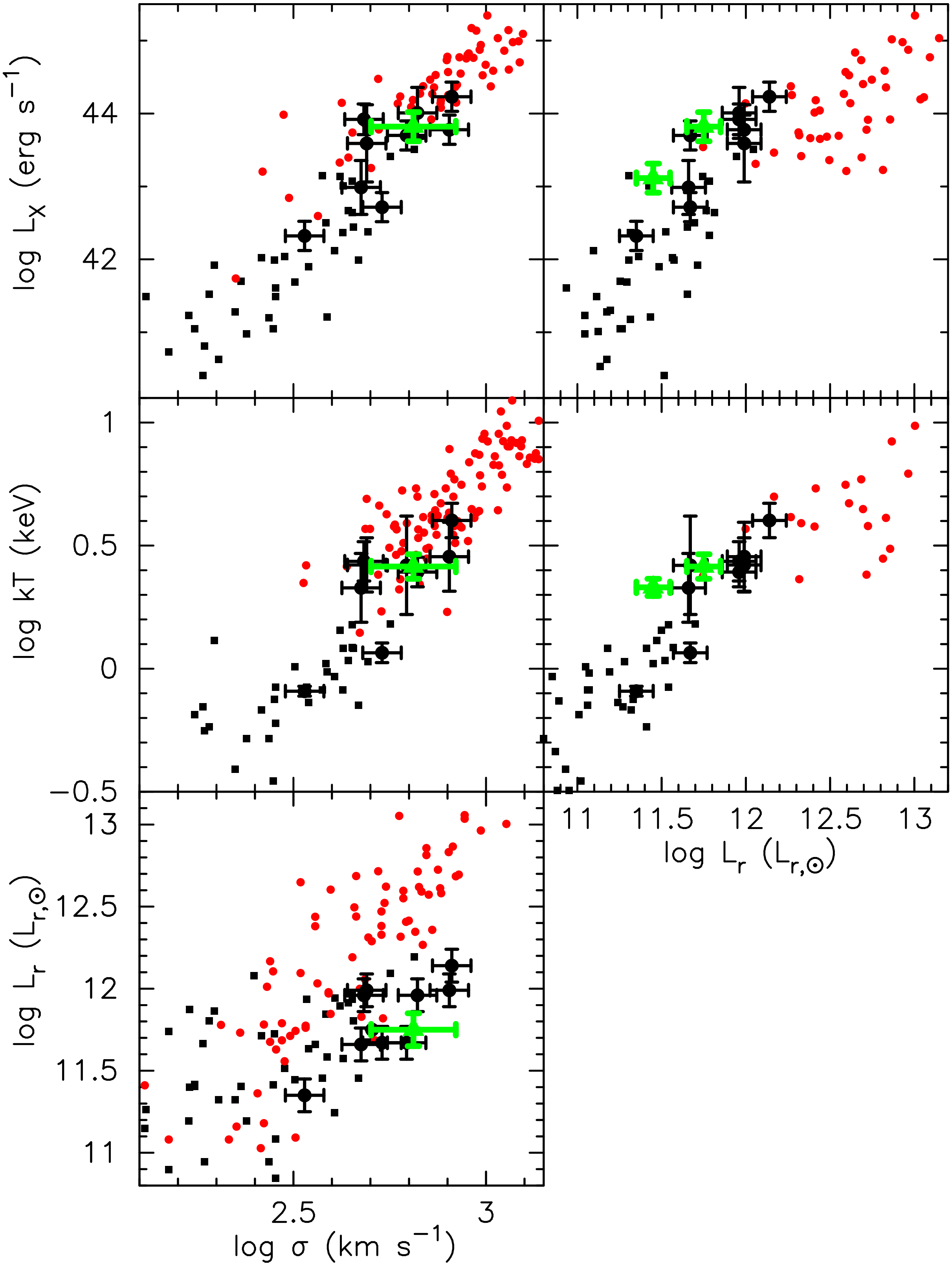

Figure 5. The scaling relations of our sample of fossil groups is compared to "normal" systems from the literature. The data presented in paper are shown as black dots with error bars. Three groups from KPJ07 are shown as green dots with error bars. Samples of "normal" groups and clusters are shown as black and red dots without error bars, respectively.

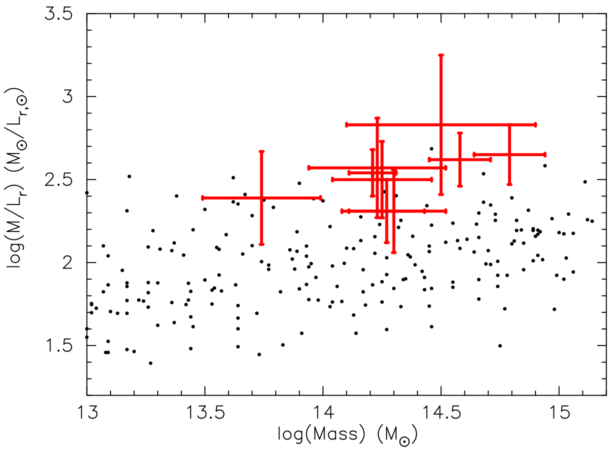

Figure 6. Mass-to-light ratios are plotted against mass (with both parameters estimated within R_{200}). Literature values for normal groups and clusters (Girardi et al., 2002) are shown as black dots.

4.4 Optical properties

In this section we look in detail at the optical properties of our fossil systems (luminosities, luminosity functions and m_{12} gaps). The data are presented in Table 3

When converting galaxy luminosities between wavebands values of $B-R$, $B-r$ and $r-i$ were taken to be 1.57, 1.33 and 0.4 mag, respectively. To convert absolute magnitudes into solar luminosities, values of the solar B, R, r and i band absolute magnitudes were taken to be 5.48, 4.42, 4.76 and 4.58 mag, respectively.

We begin by considering the m_{12} values presented in Table 3. Two sets of values are presented, one ($m_{12,S}$) is measured within the radius used in the selection process ($R_{200,S}$), the other ($m_{12,X}$) within $R_{200,X}$. Now, we demonstrated in Section 2.4 that for our samples $R_{200,X}$ is typically ∼50% larger than $R_{200,S}$, and it can be seen from Table 3 that this results in significant reductions in the observed m_{12} in many cases. We note that this effect has been noted previously by many authors (e.g. see Santos et al., 2007; Zibetti, Pierini & Pratt, 2008; Miller et al., 2011). However, since the $R_{200,S}$–$R_{200,X}$ discrepancy appears in both the SDSS and RXJ samples, rather than discard most of these systems from the fossil group sample, we simply define the fossil groups as systems with $m_{12} > 2.0$ mag within $0.5R_{200,S}$ (which corresponds to $\sim 0.33R_{200,X}$).

Now let us consider the $m_{12,S}$–L_{bcg} data from the maxBCG catalogue. These are shown in Fig. 7 (N.B. These data are also reported, in a slightly different form, in Miller et al., 2011). In this figure, diagonal lines mark the loci of second ranked galaxies of constant luminosity. Individual data points are coloured by richness (blue for $N_{200} < 25$, red for $N_{200} > 25$; see Miller et al., 2011 for the definition of richness). The groups detailed in this work are identified with circles (the SDSS sample) and squares (the RXJ sample). It should be noted that these data were taken directly from the maxBCG catalogue. The BCG luminosities are therefore not scaled to the cosmology generally used in this paper.

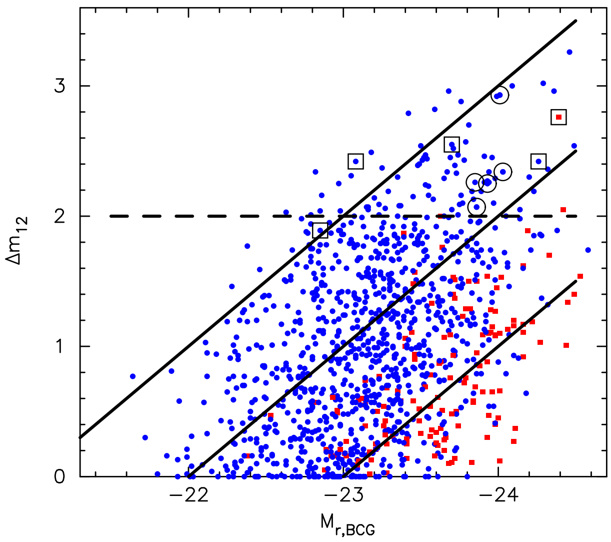

Figure 7. The luminosity gap ($m_{12,S}$) is plotted against BCG absolute magnitude. Lines of constant second ranked galaxy luminosity are marked by (diagonal) lines. These correspond to (from top to bottom) M_2=-21, -22 and -23 mag. Systems reported in this work are identified by circles (the SDSS sample) and squares (the RXJ sample). Points are coloured to indicate richness, with low richness groups ($N_{200} \leq 25$) in blue and high richness groups($N_{200} > 25$) in red.

Examination of Fig. 7 reveals three important properties of all systems exhibiting $m_{12} > 2$ mag (i.e. not just those analysed in this work):

i) Most of the BCGs in these systems are extremely bright. Indeed, many are amongst the brightest in the whole sample, and very few systems exhibit $M_{r,BCG} > -23$.

ii) Most of these systems possess very low luminosity second ranked galaxies, with very few systems exhibiting $M_{r,2} \leq -22$.

iii) Nearly all systems with $m_{12} > 2$ mag exhibit low richness. Indeed, the average richness of all systems with $m_{12} > 2$ mag is only 12.9. Only two systems with $m_{12} \geq 2$ mag exhibit $N_{200} > 25$. These include J1416, which has N_{200}=28 (and is a member of our sample), and another system with N_{200}=48.

It should be noted that the high luminosities of the BCGs in our samples are highly selection biased, as the SDSS sample was *specifically* selected to contain only systems with bright BCGs (see Section 2.1), whereas the RXJ sample was biased towards high luminosity BCGs by the selection of systems with low ratios of X-ray to BCG optical luminosity (in systems already known to be bright in the X-ray), as well as the selection of "*.......system[s] dominated by a single galaxy*".

Now, the combination of trends i) and ii) above – that FGs are found in systems with bright BCGs and low luminosity second ranked galaxies - is perhaps not surprising. However, the realisation that these high mass systems, with appropriately bright BCGs, are low richness (point iii) above) points to a novel new interpretation of these objects

An important consideration in this new interpretation of fossil systems is that there is a causal link between points ii) and iii) above. Namely, that low richness systems are *expected*, on average, to have low luminosity second rank

Table 3. The richness (N_{200}; see Miller et al., 2011), r band luminosity of the central galaxies ($L_{r,bcg}$) and the total r band luminosities within $R_{200,X}$ ($L_{r,tot}$) are given. The luminosity of the BCG is also given as fraction of the total optical light (f_{bcg}). The magnitude gaps between first and second ranked galaxies within $R_{200,S}$ – i.e. those used in the selection process - are represented by $m_{12,S}$, while the magnitude gaps found within $R_{200,X}$ are represented by $m_{12,X}$. Finally, the r band dynamical mass-to-light ratios are presented.

Group	N_{200}	log $L_{r,bcg}$ ($L_{r,\odot}$)	log $L_{r,tot}$ ($L_{r,\odot}$)	f_{bcg}	$m_{12,S}$ (mag)	$m_{12,X}$ (mag)	$\log(M_{dyn}/L_{r,tot})$ ($M_{\odot}/L_{r,\odot}$)
SDSS J0906	9	11.42	11.75	0.47	3.09	3.09	2.50 ± 0.23
SDSS J1045	13	11.44	11.96	0.30	2.00	2.00	2.62 ± 0.16
SDSS J1136	10	11.40	11.99	0.26	2.25	0.58	2.31 ± 0.25
SDSS J0856	16	11.28	11.96	0.21	2.25	1.67	2.31 ± 0.19
SDSS J1017	12	11.37	11.66	0.51	2.72	1.88	2.57 ± 0.30
RXJ J1256*	8	11.15	11.67	0.30	1.53	1.34	2.83 ± 0.42
RXJ J1331	6	10.94	11.35	0.39	1.85	1.85	2.39 ± 0.28
RXJ J1340	8	11.36	11.67	0.49	2.78	1.31	2.54 ± 0.14
RXJ J1416*	28	11.76	12.14	0.42	2.55	2.21	2.65 ± 0.18
RXJ J1552*	19	11.50	11.99	0.32	2.27	1.10	2.77 ± 0.30
Average	13	11.36	11.81	0.37	2.33	1.70	2.55

* The r band photometry of the galaxies marked by an asterisk were estimated in the i band and converted to the r band using the values given in Section 4.4.

galaxies simply due to the effect of sparse samping of the Schechter function. This effect is clearly demonstrated in the bottom panel of Fig. 10 of Hansen et al., (2005), in which the rapid decline in the number of bright galaxies present in systems as richness decreases from moderate to low values. To further demonstrate this point, in the next section we present a completeness corrected, composite luminosity function for the five systems in the SDSS sample (which, unlike the RXJ sample, have high completeness out to the virial radius).

4.5 The luminosity function

The results of our analysis of the group luminosity functions (LFs) in each of the g, r and i bands are shown in Fig. 8.

This analysis is limited by the completeness limit of the SDSS photometry of about ∼ 21 mag in the *r*-band. For the composite LF, we assume the limit to the absolute magnitude to be -18 for the g-band, and -18.5 for the r and i-band. These conservative limits were set to make sure that the individual LFs were considered inside reasonable completeness limits, before including them in the composite luminosity functions. All galaxies meeting these limits and within R_{200} of each system were included, and the LF averaged. The number of galaxies (y-axis of Fig. 8) therefore represents the number of galaxies per magnitude found within $R_{200,X}$ of a single group.

The best fit for α and M^* for the three bands are -1.08 and -20.48 mag for g, -0.95 and -21.16 mag for r and -0.97 and -21.53 mag for i. The derived LFs are shown in Fig. 8 as solid red lines. Now, the error bars on our derived LFs are large, due to the relatively small number of galaxies used in their construction. The results are therefore consistent with a broad range of literature studies. We do, however, note a particularly good agreement with the α and M^* values found by Blanton et al (2003) for the ∼150,000 galaxies in the SDSS spectroscopic survey.

As noted above, the LFs presented in Fig. 8 are the average of all the galaxies within $R_{200,X}$ of five individual groups. The y-axis of Fig. 8 therefore represents the expectation for the number of galaxies per magnitude within $R_{200,X}$ of a single group. However, we are concerned with describing the $m_{12,S}$ gaps which are defined to be within *half* of $R_{200,S}$ (which is in any case smaller than $R_{200,X}$). It is therefore necessary to apply some scaling to the derived LFs if we wish to get some idea of the LF within this much smaller region[5]. In order to estimate the required scaling we simply counted the fraction of galaxies in the SDSS sample that lie within $R_{200,X}$ and that also lie within $0.5R_{200,S}$. We find a value of 45% – i.e. 45% of galaxies included in the construction of the LFs lie within half of $R_{200,S}$. Clearly, our approach here is necessarily approximate due to the large uncertainties in α and M^*, as well as all the uncertainties inherent in our assumption of a simple scaling factor difference between LFs within $R_{200,X}$ and $0.5R_{200,S}$. Our purpose here is then *per force* simply to test the viability of our proposed re-interpretation of the FG data.

Our analysis proceeds by considering the r band properties of the five SDSS galaxies used in the construction of the LFs.

The LF resulting from the scaling of the derived r band LF by 0.45 is shown in Fig. 8 as the dashed red line. Also shown in this plot are the average luminosity of the BCGs (bold vertical line), a luminosity 2 mags fainter (thin vertical line), and the point at which the expected number of galaxies per magnitude falls below 1.0 (thin horizontal line). Now, it is evident from this plot that, over almost the entire 2 magnitude range immediately below the luminosity of the BCG, the expectation of the number of galaxies per magnitude in the scaled LF is below 1.0. This clearly indicates that m_{12} gaps are likely to be large in such low richness, bright BCG systems. The effect can be quantified by integrating along the LF over this 2 mag range. The derived value of 0.6 indicates that ∼40% of all such systems will

---

[5] The direct derivation of the LFs within this small region was not carried out, as this results in even larger errors on the derived α and M^* values

[t!]

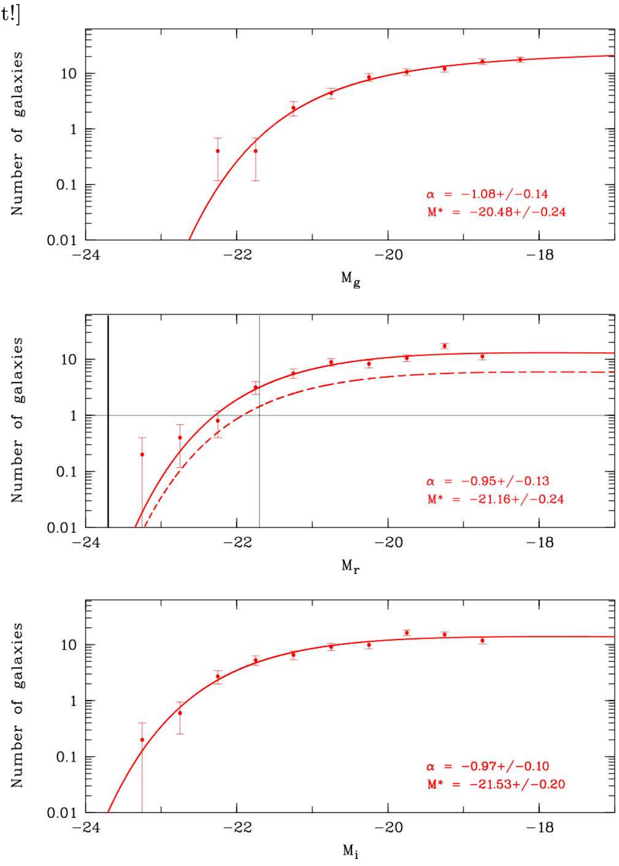

Figure 8. Composite luminosity function for four fossil groups, J0906, J1045, J0856, J1136 and J1017. The luminosity functions of each individual system are shown using differing symbols.The red line is the composite (average) luminosity function for all five systems

posses *no* galaxies within this magnitude range (and therefore possessing and $m_{121,S}$ >2.0). Now, the systems in our study were *selected* to possess $m_{121,S}$ >2.0. However, analysis of the data shown in Fig. 7 shows that, in fact 50% of the 62 low richness (N_{200} <25) systems with bright BCGs ($M_{r,bcg} < -23.5$) possess $m_{121,S}$ >2.0, in reasonably good agreement with our estimate from the r band LF of 40%.

This result is in sharp contrast with Jones et al. (2003) who performed Monte Carlo simulations using the LF of MKW/AWM clusters from Yagamata & Maehara (1986), finding an extremely low incidence of systems with m_{12} >2.0 mag. However, it is not clear from their paper what value of BCG luminosity was used. We therefore performed our analysis again, this time using the Yagamata & Maehara values for M^*, α and L_{bcg} (-21.57 mag, -1.07 and -23.0 mag, respectively). Our analysis indicates that using these values the expectation of the number of galaxies within 2 magnitudes of the BCG is 3.4. We therefore confirm that such an analysis results in extremely low probabilities of finding fossil groups. Indeed, assuming simple Poisson statistics the average of 3.4 galaxies within 2 magnitudes of the BCG would suggest fossil systems with m_{12} >2.0 mag to be 2σ events, consistent with the low numbers

The cause of the disparity between the Jones et al. results and ours is essentially the difference in the gaps between M^* and L_{bcg} which is 2.5 mag in our study, but only 1.5 mag in the Yagamata & Maehara data. We therefore conclude that the Jones et al., (2003) analysis failed to take into account the extremely bright BCGs found in fossil systems.

In summary, our analysis shows that large m_{12} gaps are an expected feature in low richness systems that host bright BCGs, and that this effect alone can account for the properties of the fossil systems in our study, without recourse to additional processes such as dynamical friction.

4.6 Synthesis

In this section we draw together the various strands of our analysis in order to gain a clearer insight into the nature of the fossil systems that we have investigated, and to identify outstanding issues.

First, let us recall the two most important conclusions of our analysis of the scaling relations of fossil system. Namely, that these systems possess high masses and, despite the high luminosities of their BCGs, low *total* optical luminosities (Section 4.3).

Considering the bright BCG luminosities and high system masses; examination of the plot of BCG luminosity against mass (M_{200}) in Hansen et al., (2009; their Fig. 13), it can be seen that the values found for our fossil groups (average $L_{bcg}=2.3\times10^{11}$ $L_\odot$, $M_{200}=2.3\times10^{14}$ $M_\odot$) are consistent with values found for normal systems in the SDSS. Indeed, the Hansen et al., plot indicates that, for a mass of 2.3×10^{14}, a typical BCG luminosity is 2×10^{11} (after the Hansen et al. data is adjusted to the cosmology used in this work). In other words, the BCG luminosities in these fossil systems are entirely consistent with their masses, but are inconsistent with either their richnesses or total optical luminosities.

The difference between fossils and normal systems can also be seen by examining the the plot of the fraction of optical light in the BCG (f_{bcg} in our Table 3) to M_{200} of SDSS groups and clusters as shown in the top panel of Fig. 14 of Hansen et al., (2009). For masses appropriate for our sample, this plot shows that normal systems with masses appropriate to our fossil sample (2.3×10^{14} $M_\odot$) possess f_{bcg} $\approx$0.12 (again after the Hansen et al. data is adjusted to the cosmology used in this work). Comparison of this value to the value of 0.37 found in fossil systems therefore again suggests a factor ~3 under-luminosity in fossils systems compared to normal systems, consistent with the value found by consideration of the L_r–σ plot (Fig. 5 and Section 4.3).

Now, given that we find the luminosities of the BCGs to be comparable between fossil and normal samples of the same mass, the discrepancy in the optical luminosity must be due to a significant under-abundance of *non*-BCG galaxies. Indeed, simple arithmetic shows that if the whole deficit is due to the lack of non-BCG galaxies, then, in order that the *total* luminosity be ~3 times lower than normal systems, fossil must contain less than 25% of the non-BCG galaxies found in a normal cluster of the same mass.

5 DISCUSSION

The picture painted by our analysis can then be summarised as follows: Fossil groups (defined as systems with $m_{12} > 2$) differ significantly from non-fossils systems of the same mass *only* in that they exhibit a large under-abundance of non-BCG galaxies. We note that this description is highly efficient in that it simultaneously describes the similarities and differences between fossil and normal systems for a host of observables (e.g. N_{200},m_{12},L_{bcg},L_{tot},L_X,T_X,σ)

In the light these conclusions, a number questions (but, unfortunately, not many answers) immediately present themselves;

- *Where are all the missing bright baryons?*
There are three immediately apparent ways to account for the "missing" baryons:

i) They have been expelled from the system (perhaps in the event of the formation of the bright BCG).

ii) They are "hidden" – possibly locked up in the hot X-ray gas, the warm/hot intergalactic medium (WHIM), or even in intra-cluster light.

iii) They were never present at all, with the systems forming in regions of space deficient in baryons (although it is difficult to see how the bright BCGs could have formed in such circumstances).

Clearly, this is an important issue that requires extensive research if it is to be resolved.

- *Are fossils really fossils? I.e. are they truly* old*?*
It is difficult to see how such low mass-to-light systems could have formed *recently*. Significant merger/accretion activity would also seem to be ruled out as this would have both ameliorated the high mass-to-light ratios and provided a significant source on non-BCG galaxies (the one thing above all else that these systems lack). It therefore seems safe to conclude that these are indeed ancient systems, and that they are indeed worthy of the title *fossil* groups.

- *What do our results mean for studies that utilise cosmological N-body/semi-analytic modeling to address issues surrounding fossil groups?*
As far as the authors are aware, no such study to-date has identified fossils as being associated with low richness systems. Whether this is a failure of the studies themselves or rather represents a failure in the baryonic physics in the semi-analytical models used in the cosmological simulations remains to be seen.

- *By what mechanism can the BCGs in the low richness systems of fossil groups achieve the same mass as those in much richer systems?*
Our results appear to present a challenge to the currently accepted paradigm of BCG formation through hierarchical clustering within the host halo (e.g. de Lucia & Blaizot 2010), as the fossil systems in our work appear to have possessed extremely low numbers of non-BCG galaxies over the whole of their lifetimes, and should therefore have been relatively starved of the raw material necessary for such a hierarchical assembly path.

All of these issues clearly need addressing in the near future if we are to establish a coherent picture of how the formation of fossil systems differs from normal systems.

6 CONCLUSIONS

We present a kinematic analysis of ten fossil group candidates, five of which have been previously identified as fossil groups in the literature. The other five candidates investigated were optically selected from the maxBCG catalogue of Koester et al. (2007), spectroscopically observed with the Magellan IMACS instrument and followed up with Chandra X-ray snapshot observations. For these 10 groups, between 10 and 64 galaxies (with an average of ∼33) are confirmed as group members within R_{200}. This study therefore represents the deepest study of a significant number of fossil systems to-date.

We confirm previous findings that the majority of the FGs in our sample lie in the regions of X-ray luminosity, X-ray temperature and velocity dispersion scaling relations occupied by galaxy *clusters* rather than groups.Since all three of these parameters (L_X, T_X and σ) can be used as proxies for mass, and all three yield masses consistent with cluster masses ($\sim10^{14}$, or greater), we can be confident in our mass estimates. We find that the luminosities of the brightest cluster galaxies in our sample are also consistent with these high masses, lending further support to this finding.

There is one parameter, however, that is *not* consistent with cluster values – namely the total optical luminosities of these systems. We find that the fossil groups are on average under-luminous by a factor ∼3 with respect to galaxy clusters of the same mass. High mass-to-light ratios has been noted in previous works (see for instance Jones et al., 2003; Yoshioka et al., 2004; KPJ07), but no firm conclusions were drawn in these works. Here, however, we find this to be essentially the defining feature of fossil systems, showing that these systems are characterised by their possession of less than 25% of the non-BCG galaxies found in normal systems of the same mass. We show that this low richness simultaneously accounts for the large m_{12} gaps *and* the high mass-to-light ratios.

We note that the *none* of the paradigms for the formation of fossils (and particularly the paradigm of cannibalism of bright central galaxies by the BCG) predict such high masses coupled with low luminosities. Our findings therefore indicate that a new paradigm for the formation and evolution of fossil groups is required.

References

Beers T.C., Flynn K., Gebhardt K., 1990, AJ, 100, 32

Bertin E., Arnouts S., 1996, A&AS, 117, 393

Blanton et al., 2003, AJ, 592, 819

Carlberg R.G., Yee H.K.C., Ellingson E., Morris S.L., Abraham R., Gravel P., Pritchet C.J., Smecker-Hane T., Hartwick F.D.A., Hesser J.E., Hutchings J.B., Oke J.B., 1997, ApJ, 485, L13

Cypriano E.S., Mendes de Oliveira C.L., Sodré L., Jr. 2006, AJ, 132, 514

Dariush A.A., Khosroshahi H.G., Ponman T.J., Pearce F., Raychaudhury S., Hartley W., 2007, MNRAS, 382, 433

Dariush A.A., Raychaudhury S., Ponman T.J., Khosroshahi H.G., Benson A.J., Bower R.G., Pearce F., 2010, MNRAS, 405, 1873

de Lucia G., Blaizot J., 2007, MNRAS, 375, 2

D'Onghia E., Sommer-Larsen J., Romeo A.D., Burkert A., Pedersen K., Portinari L., Rasmussen J., 2005, ApJ, 630, L109

Fujita Y., 2004, PASJ, 56, 29

Girardi M., Giuricin G., Mardirossian F., Mezzetti M., Boschin W., 1998, ApJ, 505, 74

Girardi M., Manzato P., Mezzetti M., Giuricin G., Limboz F., 2002, ApJ, 569, 720

Gunn J.E., Gott J.R., 1972, ApJ, 176, 1

Hansen S.M., McKay T.A., Wechsler R.H., Annis J., Sheldon E.S., Kimball A., 2005, ApJ, 633, 122

Hansen S.M., Sheldon E.S., Wechsler R.H., Koester B.P., 2009, ApJ, 699, 1333

Helsdon S.F., Ponman T.J., 2003, MNRAS, 340, 485

Jones L.R., Ponman T.J., Horton A., Babul A., Ebeling H., Burke D.J., 2003, MNRAS, 343, 627

Kawata D., Mulchaey J. S., ApJ, 672, L103

Khosroshahi H.G., Ponman T.J., Jones L.R., 2006, MNRAS, 372, 68

Khosroshahi H.G., Ponman T.J., Jones L.R., 2007, MNRAS, 377, 595 (**KPJ07**)

Koester et al., 2007, ApJ, 660, 239

Landolt A.U., 1992, AJ, 104, 340

Mendes de Oliveira C.L., Cypriano E.S, Sodré, L., Jr. 2006, AJ, 131, 158

Mendes de Oliveira C.L., Cypriano E.S., Dupke R.A., Sodré L., Jr. 2009, AJ, 138, 502

Miller et al. 2011

Maurogordato S., Sauvageot J.L., Bourdin H., Cappi A., Benoist C., Ferrari C., Mars G., Houairi K., 2010, A&A, submitted (astro-ph:1009.1967)

Navarro J.F., Frenk C.S., White S.D., 1995, MNRAS, 275, 720

Osmond J.P.F., Ponman T.J., 2004, MNRAS, 350, 1511

Ponman T.J., Allan D.J., Jones L.R., Merrifield M., McHardy I.M., Lehto H.J., Luppino G.A., 1994, Nature, 369, 462

Popesso P., Biviano A., Böhringer H., Romaniello M., 2007, A&A, 464, 451

Ramella M., Boschin W., Geller M.J., Mahdavi A., Rines K., 2004, AJ, 128, 2022

Rasmussen J., Ponman T.J., Mulchaey J.S., 2006, MNRAS, 370, 453

Santos W.A., Mendes de Oliveira C., Sodr L., Jr. 2007, AJ, 134, 1551

Schechter P., 1976, ApJ, 203, 297

Smith G.P., Khosroshahi H.G., Dariush A., Sanderson A.J.R., Ponman T.J., Stott J.P., Haines C.P., Egami E., Stark D.P., 2010, MNRAS, 409, 169

Vikhlinin A., McNamara B.R., Hornstrup A., Quintana H., Forman W., Jones C., Way M., 1999. ApJ. 520, L1 Voevodkin A., Borozdin K., Heitmann K., Habib S., Vikhlinin A., Mescheryakov A., Hornstrup A., Burenin R., 2010, ApJ, 708, 1376

Wu X.-P., Xue Y.-J., Fang L.-Z., 1999, ApJ, 524, 22

Yagamata T., Maehara H., 1986, PASJ, 38, 661

Yoshioka T., Furuzawa A., Takahashi S., Tawara Y., Sato S., Yamashita K., Kumai Y., 2004, 2004, Advances in Space Research, 34, 2525

Zhang Y.-Y., Andernach H., Caretta C.A., Reiprich T.H., Böhringer H., Puchwein E., Sijacki D., Girardi M., 2010, A&A, submitted (arXiv:1011.3018)

Zibetti S., Pierini D., Pratt G.W., 2009, MNRAS, 392, 525

Acknowledgments

This work is based on observations made with the 6.5 m Magellan/Baade telescope, a collaboration between the Observatories of the Carnegie Institution of Washington, University of Arizona, Harvard University, University of Michigan, and Massachusetts Institute of Technology, and at Cerro Tololo Inter-American Observatory, a division of the National Optical Astronomy Observatories, which is operated by the Association of Universities for Research in Astronomy, Inc. under cooperative agreement with the National Science Foundation. The COSMOS pipeline supplied by the Magellan consortium was used for data reductions. This research also made use of NASA's Astrophysics Data System, as well as IRAF and STARLINK software. IRAF is distributed by the National Optical Astronomy Observatories, which is operated by the Association of Universities for Research in Astronomy, Inc. (AURA) under cooperative agreement with the National Science Foundation. Also presented are observations obtained at the Gemini Observatory, which is operated by the Association of Universities for Research in Astronomy, Inc., under a cooperative agreement with the NSF on behalf of the Gemini partnership: the National Science Foundation (United States), the Science and Technology Facilities Council (United Kingdom), the National Research Council (Canada), CONICYT (Chile), the Australian Research Council (Australia), Ministério da Ciência e Tecnologia (Brazil) and Ministerio de Ciencia, Tecnología e Innovación Productiva (Argentina). R.A.D acknowledges support from NASA Grant NNH10CD19C and partial support from Chandra Award No. GO9-0142A. R.L.O acknowledges financial support from the Brazilian agency FAPESP (Fundação de Amparo à Pesquisa do Estado do São Paulo) through a Young Investigator Program (numbers 2009/06295-7 and 2010/08341-3). R.N.P. also acknowledges financial support from the Brazilian agency FAPESP (program number 2008/57331-0). E.S.C. also acknowledges FAPESP (program number 2009/07154-8-0) and CNPq.